Mechanics of Materials 71 (2014) 85–100

Contents lists available at ScienceDirect

Mechanics of Materials

journal homepage: www.elsevier.com/locate/mechmat

A multiscale model for reversible ferroelectric behaviour of polycrystalline ceramics

L. Daniel [a,b,*], D.A. Hall [a], P.J. Withers [a]

[a] School of Materials, University of Manchester, Grosvenor St, M13 9PL Manchester, UK
[b] LGEP – CNRS (UMR8507)/SUPELEC/UPMC/Univ Paris-Sud, 11 rue Joliot Curie, 91192 Gif-sur-Yvette, France

ARTICLE INFO

Article history:
Received 27 August 2013
Received in revised form 19 December 2013
Available online 31 January 2014

Keywords:
Domain switching
Ferroelectricity
Ferroelasticity
Self-consistent model
Residual stresses
Actuator

ABSTRACT

A multiscale model for the behaviour of ferroelectric polycrystalline materials under electro-mechanical loading is proposed. It is based on an energetic description of the equilibrium at the single crystal scale using a statistical estimate of the ferroelectric domain structure. A self-consistent scheme is then used to establish the behaviour of polycrystalline materials. The approach is anhysteretic but hysteresis effects can be added afterwards so as to obtain *butterfly* ferroelectric loops. It is applied to a tetragonal Lead Zirconate Titanate (PZT). The model allows the investigation of crystallographic texture effects on the overall behaviour and provides an estimate of internal stresses within the material. By way of an example a ⟨100⟩ fibre texture is predicted to generate as much as 150% more longitudinal strain and 33% more electric induction at 1 MV/m compared to an isotropic polycrystal.

1. Introduction

Ferroelectric ceramic materials are used extensively as dielectric and semi-conducting components, memory elements, and piezoelectric sensors, actuators and transducers. The most popular types of ferroelectric ceramics are perovskite compounds and their solid solutions such as $BaTiO_3$, Pb (Zr_xTi_{1-x}) O_3 (PZT), (Na_xK_{1-x}) NbO_3 and $(Bi_{0.5}Na_{0.5})$ TiO_3. Distortion of the parent cubic state occurs to produce a spontaneous polarisation orientated along any of the six equivalent ⟨100⟩ directions for tetragonal, twelve ⟨110⟩ directions for orthorhombic, or eight ⟨111⟩ directions for rhombohedral symmetry. Subsequently, ferroelectric or ferroelastic domain switching is accomplished by reorientation of the polarisation through 180° (all structures), 90° (tetragonal), 60°/120° (orthorhombic) or 71°/109° (rhombohedral). Recent research (Noheda et al., 1999) has suggested that other types of crystal symmetry (e.g. monoclinic) may occur for compositions close to a phase boundary, which could help to explain the high intrinsic piezoelectric activity of such materials (Guo et al., 2000). However, it is also argued that the extrinsic contributions to the piezoelectric coefficients are enhanced near to a phase boundary due to the formation of nanoscale domain structures (Schönau et al., 2007; Pramanick et al., 2011). The occurrence of domain structures in polycrystalline ferroelectrics is driven by minimisation of the energies associated with electric depoling fields and elastic residual stresses that arise on cooling through the paraelectric to ferroelectric phase transformation (Arlt, 1990). Subsequent reorientation of domains by electrical poling is necessary to impart a state of remanent polarisation and hence to obtain useful piezoelectric and pyroelectric properties in bulk ferroelectric ceramics. Furthermore, domain wall vibration and translation or localised domain switching mechanisms make significant contributions to the nonlinear dielectric,

* Corresponding author at: LGEP – CNRS(UMR8507)/SUPELEC/UPMC/Univ Paris-Sud, 11 rue Joliot Curie, 91192 Gif-sur-Yvette, France. Tel.: +33 1 69 85 16 39; fax: +33 1 69 41 83 18.
E-mail address: laurent.daniel@u-psud.fr (L. Daniel).

http://dx.doi.org/10.1016/j.mechmat.2014.01.006
0167-6636/

elastic and piezoelectric properties of poled polycrystalline ferroelectrics (Arlt, 1987; Damjanovic and Demartin, 1996; Hall and Stevenson, 1999). Control of these extrinsic contributions is carried out routinely by industry in order to develop commercial piezoceramics that exhibit properties tailored to specific applications (Berlincourt, 1992).

Considerable effort has been directed towards models that describe the properties of ferroelectric materials in order to provide accurate design tools. They result in a wide range of modelling approaches in order to define the electromechanical response of a ferroelectric material submitted to an electromechanical loading. These models mainly belong to three categories: macroscopic models, micromechanical models and domain structure models.

Macroscopic models are focused on the phenomenological description of the typical polarisation hysteresis and strain *butterfly* loops. Most of the models in the literature are based on the introduction of appropriate internal variables to describe such a behaviour. Following the early work of Chen and Peercy (1979), Maugin and co-workers developed a sound thermodynamical framework for the macroscopic description of ferroelectric behaviour (Bassiouny et al., 1988; Bassiouny et al., 1988; Bassiouny and Maugin, 1989; Bassiouny and Maugin, 1989). This approach is inspired by metal plasticity models with the use of dissipation potentials. It has further been developed by numerous authors (Kamlah and Tsakmakis, 1999; Cocks and McMeeking, 1999; Huber and Fleck, 2001; Landis, 2002; McMeeking and Landis, 2002; Elhadrouz et al., 2005a; Klinkel, 2006; Mehling et al., 2007). The objective of macroscopic models is an accurate description of ferroelectric behaviour and an easy implementation into numerical design tools (Klinkel, 2006). A review of macroscopic models has been given by Landis (2004). Some limitations of these models are that they do not provide an insight into the physical mechanisms responsible for ferroelectric behaviour and their capability to describe the effect of complex loadings is often questionable. Furthermore the effect of material heterogeneity on the overall behaviour cannot be addressed. For instance, these approaches do not consider the effect of residual stresses, although they have long been recognised as an important influence on the properties of ferroelectric ceramics (Buessem et al., 1966; Buessem et al., 1966; Arlt et al., 1985). These internal stresses are created by the manufacturing process, material heterogeneity or by the evolving ferroelectric domain structure. Moreover the input parameters for phenomenological models have to be determined by experimental measurements, and they cannot predict the influence of a change in microstructural parameters on the macroscopic ferroelectric behaviour.

In order to overcome such shortcomings, micromechanical approaches have been developed extensively over the last two decades. Inspired by the micro-mechanical models for plastic behaviour, these models consist of a local constitutive law for ferroelectric single crystals linked to scale transition rules to describe the behaviour of polycrystalline materials. For single crystal behaviour, domain variants are introduced, each corresponding to a given orientation of the polarisation. The volume fraction of each variant then becomes an internal variable. A switching criterion is then defined to describe, in a statistical way, the evolution of the microstructure under electro-mechanical loading. The switching criterion being defined, the polycrystal behaviour is described based on the localisation-homogenisation rules in order to define how the single crystal interacts with the surrounding material. Early approaches described a grain as a single domain switching as a whole (Hwang et al., 1995; Hwang et al., 1998; Michelitsch and Kreher, 1998; Chen and Lynch, 1998; Lu et al., 1999). More realistic models of progressive switching have been later developed in order to consider the possible coexistence of two domain variants (Rödel and Kreher, 2000), or the coexistence of all possible variants in a single crystal (Li and Weng, 1999; Huber et al., 1999; Huber and Fleck, 2001; Elhadrouz et al., 2005b; Shilo et al., 2007). The local electro-mechanical loading at the single crystal scale can be defined by several means. Uniform stress and electric field can be considered (Hwang et al., 1995; Hwang et al., 1998; Michelitsch and Kreher, 1998; Lu et al., 1999). Homogenisation tools can also be used to estimate the electric field and stress within the material. The self-consistent scheme derived from the description of plasticity of polycrystals by Hill (1965) is usually recognised as the most suitable for polycrystals (Huber et al., 1999; Rödel and Kreher, 2000; Huber and Fleck, 2001). Other authors made the choice of the finite element method to estimate these fields fluctuations (Hwang and McMeeking, 1999; Li and Fang, 2004; Kamlah et al., 2005; Haug et al., 2007; Pathak and McMeeking, 2008). Reviews on micromechanical modelling of ferroelectrics can be found in Landis (2004) and Huber (2005).

The need for a deeper understanding of ferroelectric behaviour and the pursuit of engineered domain configurations to enhance ferroelectric properties motivated the development of microscopic models describing domain microstructure evolution. These models are either founded on simplified domain configurations (Li and Liu, 2004; Rödel, 2007; Tsou and Huber, 2010) or exploit the domain compatibility conditions to describe the evolving domain structure (Loge and Suo, 1996; Yen et al., 2009; Weng and Wong, 2009). Another approach relies on phase field theory to define the local orientation of the polarisation (Chen, 2002; Choudhury et al., 2005; Su and Landis, 2007). The use of atomic-scale finite element method has also been proposed (Zhang et al., 2012). A review on domain evolution models has recently been undertaken by Potnis et al. (2011). These approaches provide a deep insight into the basic physical mechanisms of domain switching but are often limited to 2D configurations and incur heavy computational costs.

The model presented in this paper lies within the family of micro-mechanical approaches. The novelty stands in its formulation inspired from ferromagnetic models rather than crystalline plasticity. This formulation is derived from the micro-mechanical approaches developed in the context of magneto-elasticity (Armstrong, 1997; Buiron et al., 1999; Armstrong, 2002; Daniel et al., 2008). Compared with previous micro-mechanical approaches for ferroelectric behaviour, the proposed model does not rely on plasticity theory and does not make use of fictitious hardening parameters for the polarisation process (Huber et al., 1999).

Such hardening parameters are introduced in micromechanical models to regularise the computation, and can be the source of calculation convergence issues if chosen too small. Moreover it imposes the use of an incremental definition of the material response with small calculation steps associated with large computation time. Because the proposed approach does not require an incremental formulation the calculation can be much faster if the response of the material is sought only for a limited number of loading points. The counterpoint is that the model is anhysteretic, meaning that no description of the local hysteresis effects is given. Hysteresis effects can be computed afterwards through a phenomenological approach. Another drawback of most previous micromechanical models is that once the material is fully polarised, transverse domains cannot re-appear when the field is reversed. As already proposed by some authors (Buiron et al., 1999; Arockiarajan et al., 2007; Tang et al., 2009), the introduction of a probability function to describe the evolution of domain structure can address this limitation. The main advantage of the proposed approach, in addition to its non-incremental formulation, is its ability to describe texture effects, and local stress contributions.

In Section 2 the model for the anhysteretic ferroelectric behaviour of single crystals is detailed. The extension to polycrystalline behaviour, based on a self-consistent approach, is then proposed in Section 3. In Section 4 the model is applied to single crystal, isotropic polycrystal and textured polycrystal of a representative tetragonal PZT. A discussion on anhysteretic behaviour and possible extensions to dissipative behaviour is finally proposed.

2. Local equilibrium at the single crystal scale

A ferroelectric single crystal is divided into ferroelectric domains. It is described as a set of K domain families each corresponding to a given local polarisation $\mathbf{P}_\alpha$. For example, $K = 6$ for tetragonal materials ($\boldsymbol{\alpha}$ corresponding to the six $\langle 1\,0\,0\rangle$ directions) and $K = 8$ for rhombohedral materials ($\boldsymbol{\alpha}$ corresponding to the eight $\langle 1\,1\,1\rangle$ directions). In each domain, the polarisation $\mathbf{P}_\alpha$ is uniform and aligned with an easy axis $\boldsymbol{\alpha}$ (Eq. (1)).

$$\mathbf{P}_\alpha = P_0\,\boldsymbol{\alpha} \tag{1}$$

P_0 is the magnitude of the spontaneous polarisation of a ferroelectric domain. Each domain also undergoes a uniform ferroelectric strain $\boldsymbol{\varepsilon}^{fe}_\alpha$. Assuming that this ferroelectric strain is isochoric (Cao and Evans, 1993), the ferroelectric strain tensor can be written as a function of the saturation ferroelectric strain λ^{fe}_0 (Eq. (2)).

$$\boldsymbol{\varepsilon}^{fe}_\alpha = \frac{3}{2}\lambda^{fe}_0\left(\boldsymbol{\alpha}\otimes\boldsymbol{\alpha} - \frac{1}{3}\mathbf{I}\right) \tag{2}$$

$\mathbf{I}$ is the second order identity tensor. Eq. (2) can also be written in the form of Eq. (3), δ_{ij} being the Kronecker delta.

$$(\boldsymbol{\varepsilon}^{fe}_\alpha)_{ij} = \frac{3}{2}\lambda^{fe}_0\left(\alpha_i\,\alpha_j - \frac{1}{3}\delta_{ij}\right) \tag{3}$$

λ^{fe}_0 can be obtained by measuring the saturation strain of a single crystal, or the saturation strain of an isotropic polycrystal (see Appendix F). Assuming an isochoric transformation from the cubic phase, λ^{fe}_0 can also be deduced from the parameters of the transformed crystallographic structure under no load. λ^{fe}_0 is given by Eq. (4) for tetragonal crystals (c and a are the lattice parameters) and by Eq. (5) for rhombohedral crystals (γ is the distortion angle).

$$\lambda^{fe}_0 = \frac{2(c-a)}{c+2a} \tag{4}$$

$$\lambda^{fe}_0 = \gamma \tag{5}$$

Ferroelectric single crystals are also piezoelectric so that the local electric field $\mathbf{E}_\alpha$ in a domain α induces a piezoelectric strain $\boldsymbol{\varepsilon}^{pz}_\alpha$ (Eq. (6)) and the local stress $\boldsymbol{\sigma}_\alpha$ induces a stress induced electric induction $\mathbf{D}^{pz}_\alpha$ (Eq. (7)).

$$\boldsymbol{\varepsilon}^{pz}_\alpha = {}^t\mathbf{d}^{pz}_\alpha \cdot \mathbf{E}_\alpha \tag{6}$$

$$\mathbf{D}^{pz}_\alpha = \mathbf{d}^{pz}_\alpha : \boldsymbol{\sigma}_\alpha \tag{7}$$

$\mathbf{d}^{pz}_\alpha$ is the standard piezoelectric tensor at the single crystal scale. Usual elastic and dielectric constitutive laws give the uncoupled contribution to the strain and to the electric induction (Eqs. (8) and (9)).

$$\boldsymbol{\varepsilon}^{e}_\alpha = \boldsymbol{\mathcal{S}}_\alpha : \boldsymbol{\sigma}_\alpha \tag{8}$$

$$\mathbf{D}^{e}_\alpha = \boldsymbol{\epsilon}_\alpha \cdot \mathbf{E}_\alpha \tag{9}$$

$\boldsymbol{\varepsilon}^{e}_\alpha$ is the elastic strain and $\boldsymbol{\mathcal{S}}_\alpha$ the elastic compliance fourth order tensor. $\mathbf{D}^{e}_\alpha$ is the purely dielectric induction and $\boldsymbol{\epsilon}_\alpha$ the dielectric permittivity. Eqs. (6)–(9) define the standard dielectric, elastic and piezoelectric relationships (Corcolle et al., 2008).

The total strain $\boldsymbol{\varepsilon}_\alpha$ in a domain α is then defined as the sum of the elastic, piezoelectric and ferroelectric contributions (Eq. (10)).

$$\boldsymbol{\varepsilon}_\alpha = \boldsymbol{\varepsilon}^{e}_\alpha + \boldsymbol{\varepsilon}^{pz}_\alpha + \boldsymbol{\varepsilon}^{fe}_\alpha \tag{10}$$

Similarly the total dielectric induction $\mathbf{D}_\alpha$ in a domain α is defined as the sum of the purely dielectric, piezoelectric and ferroelectric contributions (Eq. (11)).

$$\mathbf{D}_\alpha = \mathbf{D}^{e}_\alpha + \mathbf{D}^{pz}_\alpha + \mathbf{P}_\alpha \tag{11}$$

Following the approaches developed for magneto-elastic behaviour (Hubert and Schaëfer, 1998; Daniel et al., 2008), the free energy W_α of a ferroelectric domain can be defined as the sum of an electrostatic contribution W^E_α and of an elastic contribution $W^{\boldsymbol{\sigma}}_\alpha$ (Eq. (12)). Electrostatic and elastic energies are written according to Eqs. (13) and (14) respectively (see Appendix B).

$$W_\alpha = W^E_\alpha + W^{\boldsymbol{\sigma}}_\alpha \tag{12}$$

$$W^E_\alpha = -\mathbf{E}_\alpha.\mathbf{D}^*_\alpha \tag{13}$$

$$W^{\boldsymbol{\sigma}}_\alpha = -\boldsymbol{\sigma}_\alpha : \boldsymbol{\varepsilon}^*_\alpha \tag{14}$$

$\mathbf{D}^*_\alpha$ is the non-dielectric contribution to $\mathbf{D}_\alpha$ at the domain scale (comprising the sum of the piezoelectric contribution and the spontaneous polarisation) while $\boldsymbol{\varepsilon}^*_\alpha$

is the inelastic strain at the domain scale (comprising the sum of the piezoelectric strain and the spontaneous polarisation strain).

$$\mathbf{D}^*_\alpha = \mathbf{D}^{pz}_\alpha + \mathbf{P}_\alpha \tag{15}$$

$$\boldsymbol{\varepsilon}^*_\alpha = \boldsymbol{\varepsilon}^{pz}_\alpha + \boldsymbol{\varepsilon}^{fe}_\alpha \tag{16}$$

For the sake of simplicity, we will consider weak electric field and stress heterogeneity within the single crystal, so that $\mathbf{E}_\alpha$ and $\boldsymbol{\sigma}_\alpha$ can be replaced by the average values at the single crystal scale $\mathbf{E}_\chi$ and $\boldsymbol{\sigma}_\chi$ for the calculation of the free energy. The free energy of a domain family is then given by Eq. (17).

$$W_\alpha = -\mathbf{E}_\chi \cdot \mathbf{P}_\alpha - \boldsymbol{\sigma}_\chi : \boldsymbol{\varepsilon}^{fe}_\alpha - 2\mathbf{E}_\chi \cdot \mathbf{d}^{pz}_\alpha : \boldsymbol{\sigma}_\chi \tag{17}$$

W_α only depends on the electromechanical loading at the single crystal scale (average electric field $\mathbf{E}_\chi$ and stress $\boldsymbol{\sigma}_\chi$) and on material parameters (P_0, λ^{fe}_0 and $\mathbf{d}^{pz}_\alpha$).

The equilibrium of a single crystal under a given electro-mechanical loading results in a complex domain microstructure made of a large number of ferroelectric domains. In order to describe this microstructure, the volume fraction f_α of each domain family α is introduced. This internal variable has already been introduced in many previous models (Huber et al., 1999; Buiron et al., 1999). In the proposed model the volume fractions are explicitly calculated (Eq. (18)) by means of a Boltzmann probability function (Buiron et al., 1999; Daniel et al., 2008).

$$f_\alpha = \frac{\exp(-A_s.W_\alpha)}{\sum_{\alpha=1}^{K} \exp(-A_s.W_\alpha)} \tag{18}$$

A_s is an adjustment parameter. Its value can be related to the initial slope χ_0 of the polarisation curve under no applied stress (see Appendix C and Daniel et al. (2008)):

$$A_s = \frac{3\chi_0}{P_0^2} \tag{19}$$

It can be noticed that f_α naturally satisfies:

$$\sum_{\alpha=1}^{K} f_\alpha = 1 \tag{20}$$

Assuming that the domain wall volume is negligible compared to the volume of ferroelectric domains, the response of the single crystal can be obtained by an averaging operation over all the domain families. The dielectric induction and the total strain at the single crystal scale are given by Eqs. (21) and (22) respectively.

$$\mathbf{D}_\chi = \langle \mathbf{D}_\alpha \rangle_\chi = \sum_{\alpha=1}^{K} f_\alpha \mathbf{D}_\alpha \tag{21}$$

$$\boldsymbol{\varepsilon}_\chi = \langle \boldsymbol{\varepsilon}_\alpha \rangle_\chi = \sum_{\alpha=1}^{K} f_\alpha \boldsymbol{\varepsilon}_\alpha \tag{22}$$

In addition we assume that the non-dielectric part of the electric induction $\mathbf{D}^*_\chi$ and the inelastic part of the strain $\boldsymbol{\varepsilon}^*_\chi$ can be obtained from the volume average over the single crystal (Eqs. (24) and (23)). This assumption is rigorously valid only if we consider homogeneous dielectric and elastic properties within the single crystal ($\boldsymbol{\epsilon}_\alpha = \boldsymbol{\epsilon}_\chi$ and $\mathcal{S}_\alpha = \mathcal{S}_\chi$, for all α).

$$\boldsymbol{\varepsilon}^*_\chi = \langle \boldsymbol{\varepsilon}^*_\alpha \rangle_\chi = \sum_{\alpha=1}^{K} f_\alpha \boldsymbol{\varepsilon}^*_\alpha \tag{23}$$

$$\mathbf{D}^*_\chi = \langle \mathbf{D}^*_\alpha \rangle_\chi = \sum_{\alpha=1}^{K} f_\alpha \mathbf{D}^*_\alpha \tag{24}$$

3. Polycrystal behaviour

Polycrystalline behaviour can be deduced from appropriate averaging of single crystal behaviour. We adopt here the classical self-consistent scheme, known to be appropriate for polycrystalline materials (Hill, 1965; Berveiller and Zaoui, 1978; Huber et al., 1999; Daniel et al., 2008). Given the macroscopic applied stress $\boldsymbol{\sigma}_\Omega$ and electric field $\mathbf{E}_\Omega$, the electromechanical loading at the single crystal scale is defined by Eqs. (25) and (26).

$$\boldsymbol{\sigma}_\chi = \mathcal{B}^{\boldsymbol{\sigma}}_\chi : \boldsymbol{\sigma}_\Omega + \mathcal{L}^{\boldsymbol{\sigma}}_\chi : \left(\boldsymbol{\varepsilon}^*_\Omega - \boldsymbol{\varepsilon}^*_\chi\right) \tag{25}$$

$$\mathbf{E}_\chi = \mathcal{A}^E_\chi : \mathbf{E}_\Omega + \mathcal{M}^E_\chi : \left(\mathbf{D}^*_\Omega - \mathbf{D}^*_\chi\right) \tag{26}$$

$\mathcal{B}^{\boldsymbol{\sigma}}_\chi$ and $\mathcal{B}^E_\chi$ are respectively the stress and electric field concentration tensors. They account for the influence of the heterogeneity of the elastic and dielectric properties on the stress and electric field distributions within the polycrystal. $\mathcal{L}^{\boldsymbol{\sigma}}_\chi$ and $\mathcal{M}^E_\chi$ are respectively the stress and electric field incompatibility tensors. They account for the misfit between local and overall strain or dielectric induction in the creation of internal stresses and electric field. If initial intergranular stresses are pre-existing – for instance due to fabrication processes – they can also be added at this stage (Eq. (25)). The practical calculation of the localisation operators is given in Appendix D. They depend on the single crystal properties and on the material overall properties. As shown by Corcolle et al. (2008), the localisation operators in coupled electro-mechanical problems can be obtained separately from the purely elastic and purely dielectric problem. The contribution of piezoelectric effect and polarisation state to the heterogeneity of stress and electric field is then reported in the second term, introducing $\boldsymbol{\varepsilon}^*_\Omega$ and $\boldsymbol{\varepsilon}^*_\chi$, or $\mathbf{D}^*_\Omega$ and $\mathbf{D}^*_\chi$.

Once the local electromechanical loading is obtained from Eqs. (25) and (26), the free energy W_α of each domain family α is calculated (Eq. (17)) and then the volume fractions (Eq. (18)). The average response of each single crystal being known, the last step is the homogenisation transition scale to define the macroscopic response of the material (Eqs. (27) and (28)).

$$\boldsymbol{\varepsilon}_\Omega = \langle \boldsymbol{\varepsilon}_\chi \rangle_\Omega \tag{27}$$

$$\mathbf{D}_\Omega = \langle \mathbf{D}_\chi \rangle_\Omega \tag{28}$$

The inelastic part of the strain (Eq. (29)) and the non-dielectric part of the electric induction (Eq. (30)) can also be defined (Corcolle et al., 2008).

$$\boldsymbol{\varepsilon}^*_\Omega = \langle {}^t\mathcal{B}^{\boldsymbol{\sigma}}_\chi : \boldsymbol{\varepsilon}^*_\chi \rangle_\Omega \tag{29}$$

$$\mathbf{D}^*_\Omega = \langle {}^t\mathcal{A}^E_\chi \cdot \mathbf{D}^*_\chi \rangle_\Omega \tag{30}$$

The localisation operations defined by Eqs. (25) and (26) make use of the macroscopic response of the polycrystal $(\boldsymbol{\varepsilon}^*_\Omega, \mathbf{D}^*_\Omega)$ so that the procedure is self-consistent.

4. Modelling results

The proposed model is suitable for both rhombohedral and tetragonal materials. Single crystal elastic, dielectric and piezoelectric anisotropies are taken into account through the use of material properties defined at the domain scale (elastic stiffness $\mathcal{C}_\alpha$, dielectric permittivity $\boldsymbol{\epsilon}_\alpha$, piezoelectric tensor $\mathbf{d}^{pz}_\alpha$, spontaneous polarisation P_0 and ferroelectric strain λ^{fe}_0). Polycrystalline anisotropy is taken into account through the use of a discrete orientation distribution function to define grain orientations. As an illustration, the model has been applied to a single crystal, to an isotropic polycrystal and finally to a strongly textured polycrystal, all with a tetragonal structure.

The properties used for the single crystal have been taken from Kamlah and Wang (2003) to represent tetragonal Lead Zirconate Titanate (PZT) except A_s (specific to the proposed modelling). These properties are as follows. Elastic behaviour is taken as uniform within a single crystal ($\mathcal{C}_\alpha = \mathcal{C}_\chi$) and isotropic (Young's modulus $E = 60$ GPa and Poisson's ratio $\nu = 0.37$). Dielectric behaviour is taken as uniform within a single crystal ($\boldsymbol{\epsilon}_\alpha = \boldsymbol{\epsilon}_\chi$) and isotropic (dielectric permittivity $\epsilon = 0.02$ μF/m). The piezoelectric properties are transversely isotropic about the direction of the spontaneous polarisation which is expected for a tetragonal perovskite ferroelectric (Du et al., 1998; Damjanovic et al., 2002) ($d_{15} = 5.8\ 10^{-10}$ m/V, $d_{31} = -2.1\ 10^{-10}$ m/V, $d_{33} = 4.5\ 10^{-10}$ m/V). The spontaneous ferroelectric strain is $\lambda^{fe}_0 = 0.2\%$ and the spontaneous polarisation is $P_0 = 0.3$ C/m^2. The value for A_s is $A_s = 10^{-5}$ m^3/J. Using these material parameters, the role of local elastic anisotropy is neglected in the modelling. A discussion on the influence of elastic anisotropy is proposed in Appendix E.

4.1. Single crystals

Fig. 1 shows the anisotropy of the ferroelectric behaviour of the single crystal under electric field.

As expected for a tetragonal material, the ⟨100⟩ directions are the easy polarisation axes (Fig. 1(a)). Once the ferroelectric switching is totally completed the electric induction evolves linearly as a function of the electric field, consistent with a purely dielectric behaviour. The strain-electric field curves (Fig. 1(b)) also become linear when the domain switching is totally completed, corresponding to piezoelectric behaviour. For tetragonal PZT the ⟨111⟩ curve is totally linear since only 90° switching can induce ferroelectric strain, and this type of domain switching does not occur for a tetragonal material loaded along the ⟨111⟩ direction (Hall et al., 2005).

Fig. 2 illustrates the behaviour of a single crystal under combined uniaxial stress and electric field along a ⟨110⟩ direction. Due to the applied stress, the strain at zero electric field is not zero. For reading clarity, the curves of Fig. 2(b) have been shifted so that the strain at zero electric field is removed, reproducing what would be an experimental measurement for which the reference strain state is defined at zero electric field. This convention will be applied in the following for all strain curves.

Similar to the behaviour in the absence of stress, both the electric induction and the strain curves become linear as soon as the ferroelectric domain switching is completed. It is evident from Fig. 2 that the effect of stress is very significant and does not show symmetry between tension and compression. A high tensile stress completes the 90° switching so that no ferroelectric strain is added by applying an electric field and the strain curve is linear from the beginning. 180° switching remains possible – stress has no effect on 180° switching because the elastic energy is a quadratic function of $\boldsymbol{\alpha}$ – so that a change in polarisation

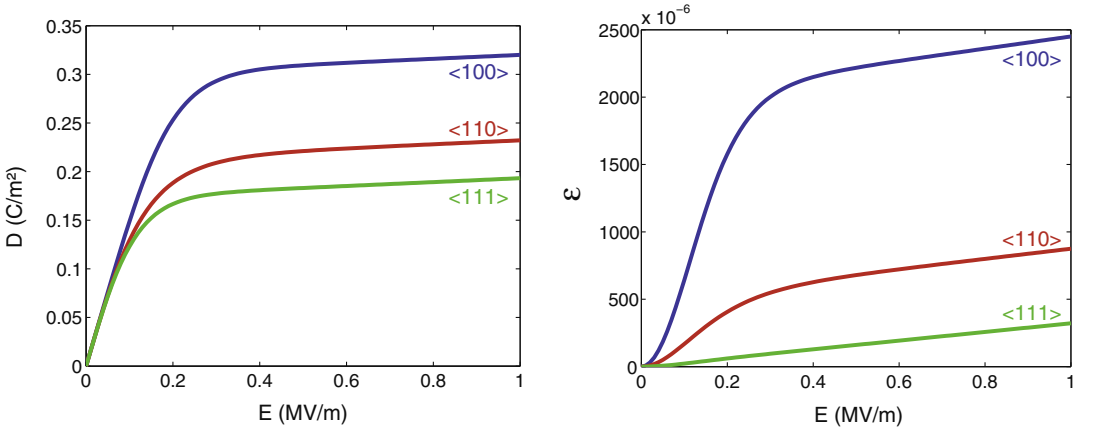

(a) Electric induction curve (b) Strain curve

Fig. 1. Directional properties of a PZT single crystal. Ferroelectric behaviour along ⟨100⟩, ⟨110⟩ and ⟨111⟩ directions in terms of (a) electric induction and (b) strain (components parallel to the applied electric field).

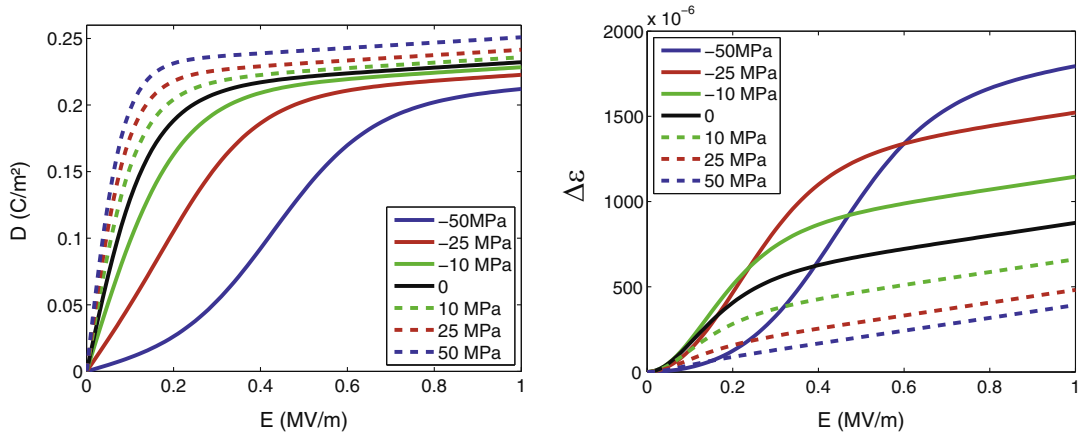

(a) Electric induction curve (b) Strain curve

Fig. 2. PZT single crystal. Ferroelectric behaviour along ⟨110⟩ direction with an applied uniaxial stress along ⟨110⟩. For clarity the strains are plotted relative to those at zero applied field.

can occur by domain switching under the application of an electric field. Under a high electric field, the difference in dielectric induction between the different loadings is due to the piezoelectric effect (term $\mathbf{D}^{pz}$).

4.2. Isotropic polycrystals

A set of crystal orientations are needed to describe a polycrystal. To approximate an isotropic polycrystal we use a regular zoning in the space of possible orientations rather than a random selection from that space. Each crystallite is defined by three Euler angles (ϕ_1, ψ, ϕ_2) following Bunge's notation. Each angle takes values regularly distributed in their domain, following Table 1.

The number of values taken in each space domain gives the precision of the texture isotropy. We use a distribution function made of 546 $(13 \times 7 \times 6)$ different orientations. The corresponding pole figures are given in Fig. 3. This approximation to isotropic texture has been used by Daniel et al. (2008) and gives representative results with a lower number of orientations than if a set of random orientations was used (see Appendix F).

Table 1
Values chosen for the Euler angle for the "isotropic" texture.

Variable	Domain	Number of values
ϕ_1	$[0, 2\pi]$	13
$\cos\psi$	$[0, 1]$	7
ϕ_2	$[0, 2\pi]$	6

Fig. 4 shows the modelling results for the ferroelectric behaviour of the isotropic polycrystal under uniaxial stress, the stress being applied in the direction parallel to the electric field. It should be noted that the model allows calculating the polycrystal response under any type of electromechanical loading and notably multiaxial stress states. It is also noteworthy that the effect of stress on ferroelectric behaviour is non-symmetric in tension/compression.

For the material studied, a tensile stress increases the amplitude of the electric induction while compression decreases it (Fig. 4(a)). The effect of stress on the strain curve is more complex to analyse (Fig. 4(b)). This effect is the result of two influences, as illustrated in Fig. 5.

Compressive stress reduces the ferroelectric strain somewhat but tensile stress significantly reduces it at high levels of electric field (Fig. 5(a)). On the other hand, the piezoelectric strain is slightly increased by a tensile stress while a compressive stress reduces it (Fig. 5(b)). The combination of these effects results in a reduction of the total strain under stress. Recall that the initial strain in the absence of electric field is removed from the total strain in the proposed figures. It can be noticed that although linear

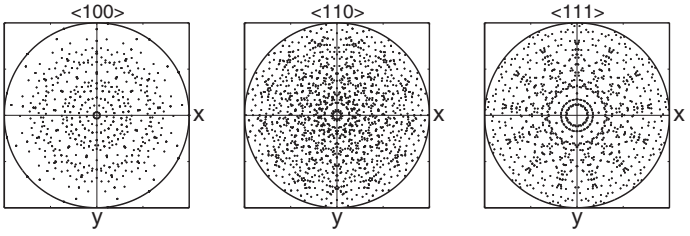

Fig. 3. ⟨100⟩, ⟨110⟩ and ⟨111⟩ pole figures for the "isotropic" polycrystal obtained by regular zoning of the crystallographic orientations space (stereographic projection, 546 orientations).

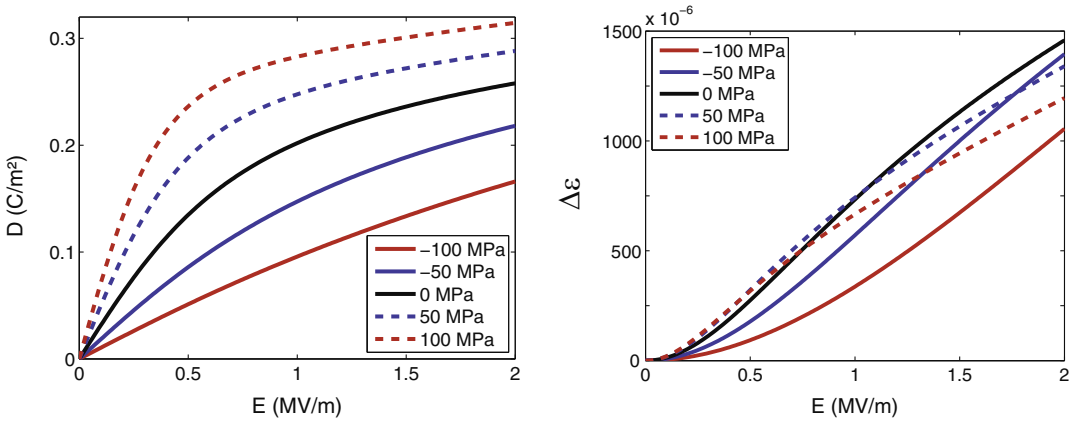

(a) Electric induction curve (b) Strain curve

Fig. 4. PZT isotropic polycrystal: anhysteretic ferroelectric behaviour under uniaxial stress along electric field direction. For clarity the strains are plotted relative to those at zero applied field.

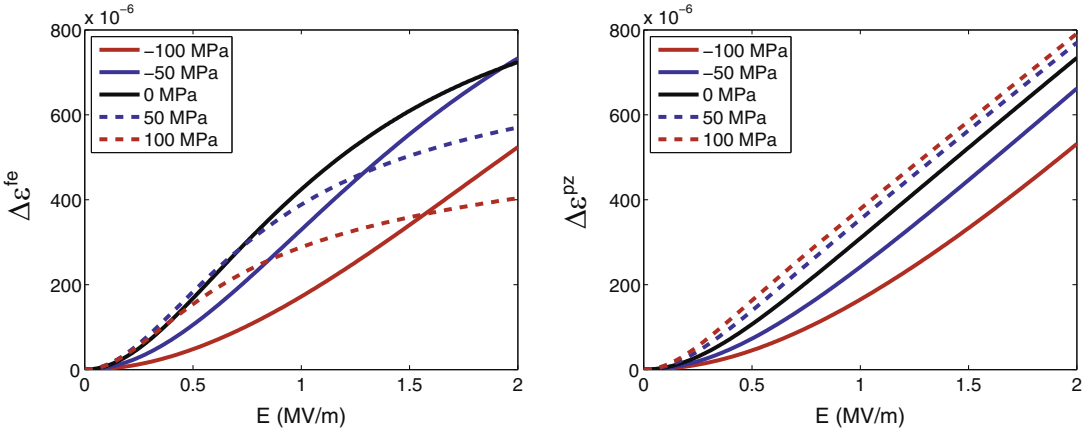

(a) Ferroelectric strain curve (b) Piezoelectric strain curve

Fig. 5. PZT isotropic polycrystal: ferroelectric and piezoelectric strain under uniaxial stress along electric field direction. For clarity the strains are plotted relative to those at zero applied field.

at the domain scale the piezoelectric strain is non linear as a function of the applied electric field. This is due to the evolving domain structure that changes the volume fraction of domains as the electric field changes.

The model also allows the extraction of the evolution of intergranular internal stresses under electromechanical loading. As an illustration, Fig. 6 shows these internal stresses in the material in the absence of applied stress for an applied electric field $E = 1$ MV/m.

The average of the internal stresses remains equal to the macroscopic stress (zero here) whatever the level of applied electric field, but the local stress levels are getting higher as the electric field increases. Fig. 7 illustrates the evolution of intergranular stress as a function of the applied electric field.

Fig. 7(a) shows the evolution of the stress second order moments within the polycrystal (components M_{12} and M_{33}, the electric field being applied along direction 3). Second order moments are the average values of the square of stress components. High second order moments indicate high heterogeneity of stress within the material. Fig. 7(b) gives the maximum value of intergranular stress within the polycrystal. Even though the average stress remains zero whatever the level of the electric field, the maximum local stresses reach significant amplitudes that could lead to fatigue and failure.

4.3. Textured polycrystals

The model allows the investigation of the effect of crystallographic texture on ferroelectric behaviour. This is of primary importance for the development of lead-free ferroelectric ceramics since the development of specific textures can enhance the ferroelectric properties, allowing lead-free materials to compete with standard lead-based ferroelectric ceramics (Hong et al., 2000; Saito et al., 2004; Rödel et al., 2009). A pure {hkl}⟨100⟩ fibre crystallographic texture aligned with the x direction has been

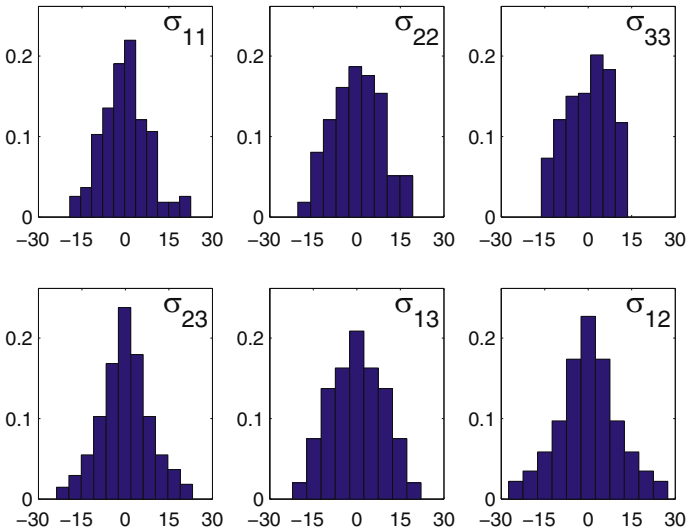

Fig. 6. Distribution of intergranular residual stress (MPa) within the polycrystal with no applied stress and an applied electric field $E = 1$ MV/m. The stress level is reported on the x-axis, and the probability on the y-axis (proportion of grains that experience a certain level of internal stress).

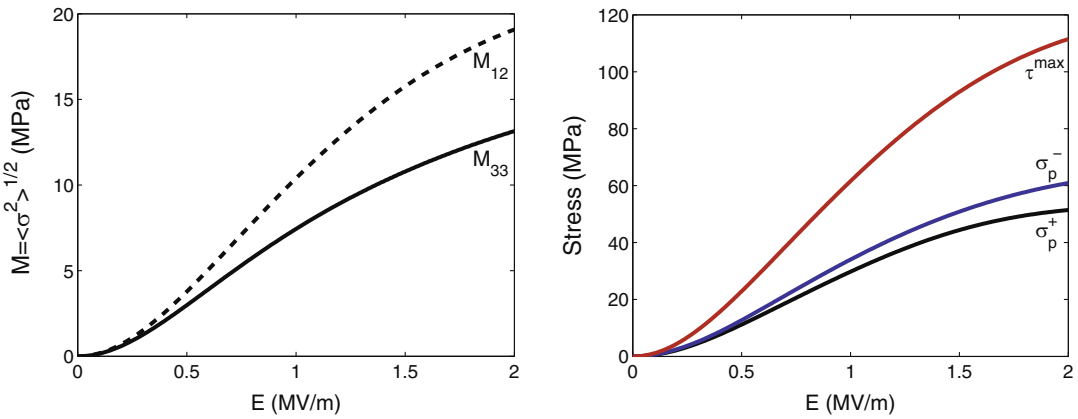

(a) Second order moments (b) Maximum stress

Fig. 7. Variability of stress and maximum values within the polycrystal as a function of the applied electric field (no applied stress). M_{ij} are the components of the second order moments of stress. $\boldsymbol{\sigma}_p^+$ is the maximum positive principal stress, $\boldsymbol{\sigma}_p^-$ is the maximum negative principal stress (absolute value) and τ^{max} is the maximum shear stress within the material.

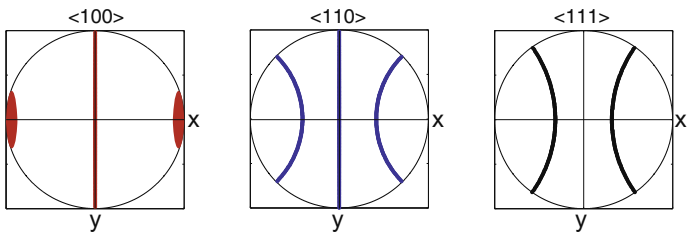

Fig. 8. ⟨100⟩, ⟨110⟩ and ⟨111⟩ pole figures for a perfect {hkl}⟨100⟩ fibre texture (stereographic projection, 90 orientations).

simulated for PZT (Fig. 8). Its behaviour along the fibre direction (x) is compared with that of the corresponding isotropic polycrystal in Fig. 9.

It is evident that the presence of a large number of ⟨100⟩ directions along the poling direction significantly enhances the permittivity. The electric induction is

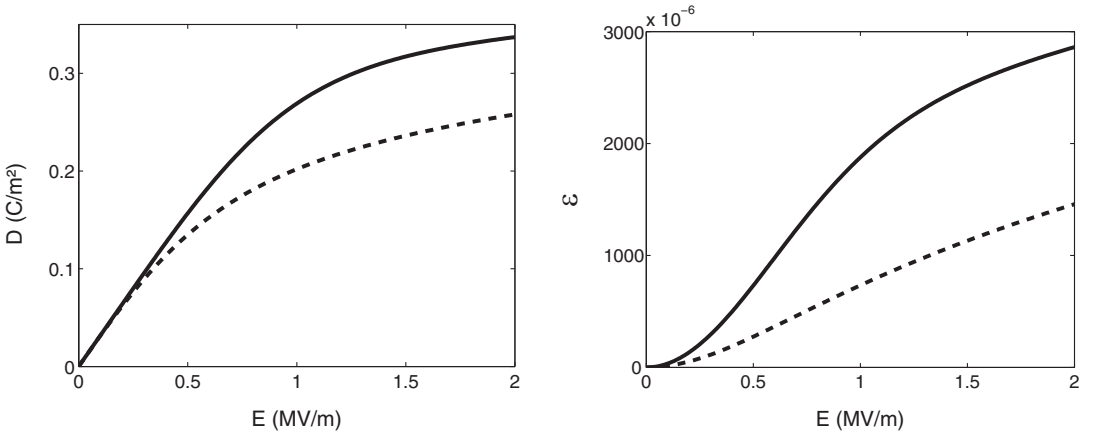

(a) Electric induction curve (b) Strain curve

Fig. 9. PZT textured polycrystal: anhysteretic ferroelectric behaviour along the *x* (fibre) direction (solid line) in the absence of applied stress compared with the corresponding isotropic polycrystal (dashed).

increased by 33% at 1 MV/m and by 30% at 2 MV/m. Texture has an even more dramatic effect on the longitudinal strain giving an increase of 156% at 1 MV/m and 96% at 2 MV/m over the isotropic case. Such a model is useful in assessing the likely rewards associated with improved texture processing of such materials.

5. Relevance and practical determination of anhysteretic curves

Anhysteretic curves describe the thermodynamic equilibrium of a material under a given external loading. They have long been used to describe the behaviour of ferromagnetic materials (Bozorth, 1951; Jiles, 1991). The proposed anhysteretic approach gives the thermodynamic equilibrium in terms of volume fractions of different domain families – or variants – for a material under a given electromechanical loading. Such an approach does not account for any cause that would prevent the domains from switching in an optimal energetic manner. Even though the role of defects or history effects are not considered, the anhysteretic curve can provide important insights into the basic mechanisms of ferroelectric behaviour under coupled loading. Anhysteretic behaviour is the idealised material behaviour, and the actual equilibrium state can be defined as a variation around this reference state.

Although it cannot be continuously described, each point of an anhysteretic curve can be measured. Two main experimental methods can be used.

The first method is to apply to the material a large amplitude alternating electric field superimposed on a dc electric field. The amplitude of the alternating field is slowly reduced to zero until only the dc field remains. The final polarisation and strain measurements provide the point of the anhysteretic curve corresponding to the applied dc field. The anhysteretic curves are obtained by repeating the operation for several dc fields. If the amplitude of the alternating field is sufficiently large, the frequency sufficiently low and the decrease of amplitude sufficiently smooth, this method provides repeatable and well defined curves. The main issue with this method is the risk of material failure due to the high number of high amplitude cycles imposed on the sample.

A second method involves heating the material below its Curie Temperature and then cooling it slowly under an applied dc field. Here again the procedure has to be applied for several dc field values to build the anhysteretic curves.

Although not exactly identical, as shown in the case of ferromagnetic materials by Pearson et al. (1997), these methods are expected to provide similar curves.

6. Introduction of hysteresis effects

The proposed model is anhysteretic, meaning that it describes the reversible part of ferroelectric behaviour. Ferroelectric behaviour is of course fundamentally hysteretic. The hysteresis effects can be added afterwards as proposed, for instance, by Jiles and Atherton (1984), or Hauser (2004) for ferromagnetic behaviour. We propose to follow here the approach of Hauser (2004). The hysteresis is introduced at the single crystal scale. The input of the calculation is still the macroscopic anhysteretic electric field $\mathbf{E}_\Omega^{an}$. Once all the internal variables have been calculated, the total electric field $\mathbf{E}_\chi^{an}$ at the single crystal scale is written according to Eq. (31).

$$\mathbf{E}_\chi^{tot} = \mathbf{E}_\chi^{an} \pm \left[1 - a\,\exp(b\,(\mathbf{P}_\chi - \mathbf{P}_\chi^{reb}))\right]\left(c + d\,|\mathbf{E}_\chi^{an}|\right) \qquad (31)$$

$\mathbf{P}_\chi^{reb}$ is the last value of $\mathbf{P}_\chi$ for which the direction of the electric field has been reversed. In contrast to the anhysteretic model, this formulation requires the implementation of an incremental formulation so that the loading history is known. Moreover it adds four adjustment parameters a, b, c and d. These four parameters can be identified from a major polarisation loop: a and d affect the general shape of the loop, b governs the stiffness of the first polarisation curve and the sharpness of the polarisation knees, and c defines the coercive field of the major loop. The macroscopic total field $\mathbf{E}_\Omega^{tot}$ is then obtained by a volume averaging over the volume of the polycrystal:

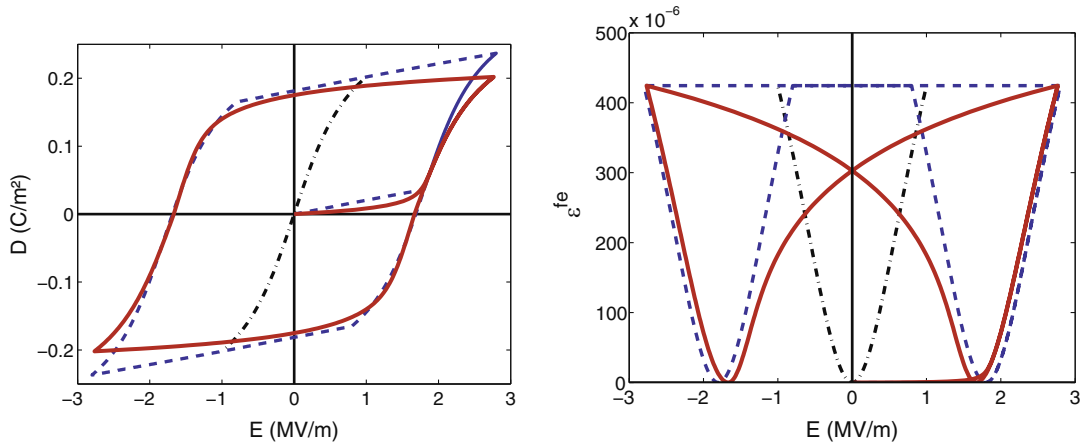

(a) Electric induction curve (b) Strain curve

Fig. 10. PZT isotropic polycrystal: Hysteresis and *butterfly* ferroelectric loops for an isotropic PZT polycrystal with the strain parallel to the electric field using the formulation given in Eq. (31) (solid line), and using the switching threshold given in Eq. (33) (dashed). The anhysteretic solution is also recalled (dashdot).

$$\mathbf{E}_\Omega^{tot} = \langle \mathbf{E}_\chi^{tot} \rangle_\Omega \tag{32}$$

This approach has been implemented for the isotropic polycrystal of Section 4.2 using a = 1.0, b = 110 m^2/C, c = 1.7 10^6 V/m and d = 0.10. The results are shown in Fig. 10 for the dielectric induction and strain under applied electric field.

Another simple way to introduce hysteresis is to introduce a switching threshold. The volume fractions f_α are then calculated not according to the local electric field $\mathbf{E}_\chi$ but to an effective electric field $\mathbf{E}_\chi^{eff}$ parallel to $\mathbf{E}_\chi$ with a magnitude E_χ^{eff} defined by Eq. (33).

$$\begin{aligned} E_\chi^{eff} &= \sup(0, E_\chi - E^Y) \text{ for the first polarisation curve} \\ E_\chi^{eff} &= E^{max} + \inf(0, E_\chi + E^Y) \text{ for decreasing electric field} \\ E_\chi^{eff} &= E^{min} + \sup(0, E_\chi - E^Y) \text{ for increasing electric field} \end{aligned} \tag{33}$$

E^Y is the threshold electric field under which no domain switching can occur. E^{max} and E^{min} are the maximum and minimum value of the electric field since last reversal of electric field direction. The corresponding results for the dielectric induction and the ferroelectric strain are plotted in Fig. 10 using a threshold E^Y = 1.8 MV/m. A stress threshold could also be introduced for domain switching under stress. In the general case of a coupled electromechanical loading, an energetic switching threshold should be defined. Such an approach has not been implemented yet and is beyond the scope of this paper focused on anhysteretic behaviour.

7. Conclusion

In this paper a novel anhysteretic multiscale model for ferroelectric behaviour has been proposed. It applies to polycrystalline ferroelectrics with tetragonal or rhombohedral crystallographic structure. It naturally includes the description of anisotropies at multiple scales – ferroelectric domain, single crystal and polycrystal scale. A discrete orientation distribution function is used as an input of the model so that the relationship between crystallographic texture and macroscopic properties can be investigated. This illustrates the potential benefits achievable by improved processing to introduce crystallographic texture in polycrystalline materials. The model also provides an estimate of intergranular internal stresses which are of primary importance for the durability of ferroelectric materials. It shows that even when the average stresses are zero, significant (up to 100 MPa) stresses are generated with increasing electric field within the grains.

The approach is restricted to anhysteretic behaviour, but it is believed that although the calculated polarisation or strain curves do not include dissipation effects, some basic mechanisms of electromechanical coupling in ferroelectric materials are captured by the model. The model gives a description of electric field and stress fluctuations within the material for a given polarisation level. Hysteresis effects can be introduced afterwards to obtain realistic strain-field *butterfly* loops at the price of an incremental formulation and increased computational cost.

Numerous validation steps remain ahead. An experimental setup is currently being designed in order to perform practical anhysteretic measurements on ferroelectric ceramics. These measurements will allow quantitative validation of the proposed model, and are expected to demonstrate the relevance of the separation between reversible and irreversible contributions to ferroelectric behaviour. Such a separation has been instrumental in the development of efficient constitutive models for ferromagnetic behaviour (e.g. Jiles and Atherton (1984) and Hauser (2004)). A comparison between the main micromechanical approaches to ferroelectric behaviour available in the literature should also be undertaken in order to highlight the respective strengths and weaknesses of models derived from plasticity theory and from ferromagnetism. This comparison should not only rely on macroscopic responses of ferroelectric ceramics subjected

to electro-mechanical loading but also on a local analysis. This local analysis can be performed using high energy X-ray diffraction measurements giving access to internal stresses and volume fractions of domains in ferroelectric ceramics (Hall et al., 2005). Such experiments can be used as a powerful tool to discriminate between micro-mechanical models. They can also be used to identify the material parameters needed to feed these multiscale approaches.

Acknowledgement

This work was supported at the University of Manchester by the Engineering and Physical Sciences Research Council (EPSRC) under the Grant EP/J010685/1. L.D. gratefully acknowledges sabbatical leave support granted by Univ Paris-Sud.

Appendix A. Nomenclature

A summary of the nomenclature used in this paper is given hereafter.

A.1. Subscripts

For state variables and material properties, subscripts define the scale at which the quantity is expressed (see Table A.2).

Table A.2
Definition of subscripts.

Subscript	Corresponding scale
α	Ferroelectric domain (microscale)
χ	Single crystal or grain (mesoscale)
Ω	Polycrystal (macroscale)

A.2. State variables

The state variables used in this paper as summarised in Table A.3.

Table A.3
State variables.

Symbol	State variable
$\boldsymbol{\varepsilon}$	Total strain tensor
$\boldsymbol{\varepsilon}^{fe}$	Ferroelectric strain tensor
$\boldsymbol{\varepsilon}^{pz}$	Piezoelectric strain tensor
$\boldsymbol{\varepsilon}^{e}$	Elastic strain tensor
$\boldsymbol{\varepsilon}^{*}$	Inelastic strain tensor
$\boldsymbol{\sigma}$	Stress tensor
$\mathbf{D}$	Dielectric induction
$\mathbf{P}$	Electric polarisation
$\mathbf{D}^{pz}$	Stress induced dielectric induction
$\mathbf{D}^{e}$	Purely dielectric induction
$\mathbf{D}^{*}$	Non-dielectric induction
$\mathbf{E}$	Electric field

A.3. Material parameters

The material parameters used in this paper as summarised in Table A.4.

Table A.4
Material parameters.

Symbol	Material parameter
P_0	Spontaneous electric polarisation
λ_0^{fe}	Spontaneous ferroelectric strain
$\boldsymbol{\epsilon}$	Permittivity tensor
$\mathbf{d}^{pz}$	Piezoelectric coefficients
$\mathcal{S}$	Elastic compliance tensor
$\mathcal{C}$	Elastic stiffness tensor ($\mathcal{C}=\mathcal{S}^{-1}$)
A_s	Adjustment parameter
χ_0	Initial slope of the macroscopic polarisation curve

Appendix B. Definition of electrostatic and elastic energies

The electrostatic energy is usually given by:

$$W_\alpha^E = \frac{1}{2}\,\mathbf{E}_\alpha \cdot \mathbf{D}_\alpha^e \tag{B.1}$$

It can be transformed as follows, noting $\boldsymbol{\nu}_\alpha$ and $\boldsymbol{\nu}_\chi$ the inverse of the Permittivity tensor at the domain scale and at the single crystal scale.

$$\begin{aligned} W_\alpha^E &= \frac{1}{2}\,\mathbf{E}_{\alpha_i}\mathbf{D}_{\alpha_i}^e = \frac{1}{2}\,\boldsymbol{\nu}_{\alpha_{ij}}(\mathbf{D}_{\alpha_i}-\mathbf{D}_{\alpha_i}^*)(\mathbf{D}_{\alpha_j}-\mathbf{D}_{\alpha_j}^*) \\ &= \frac{1}{2}\,\boldsymbol{\nu}_{\alpha_{ij}}\mathbf{D}_{\alpha_i}\mathbf{D}_{\alpha_j} + \frac{1}{2}\,\boldsymbol{\nu}_{\alpha_{ij}}\mathbf{D}_{\alpha_i}^*\mathbf{D}_{\alpha_j}^* - \boldsymbol{\nu}_{\alpha_{ij}}\mathbf{D}_{\alpha_i}\mathbf{D}_{\alpha_j}^* \\ &= \frac{1}{2}\,\boldsymbol{\nu}_{\alpha_{ij}}\mathbf{D}_{\alpha_i}\mathbf{D}_{\alpha_j} + \frac{1}{2}\,\boldsymbol{\nu}_{\alpha_{ij}}\mathbf{D}_{\alpha_i}^*\mathbf{D}_{\alpha_j}^* - \boldsymbol{\nu}_{\alpha_{ij}}(\mathbf{D}_{\alpha_i}^* + \mathbf{D}_{\alpha_i}^e)\mathbf{D}_{\alpha_j}^* \\ &= \frac{1}{2}\,\boldsymbol{\nu}_{\alpha_{ij}}\mathbf{D}_{\alpha_i}\mathbf{D}_{\alpha_j} - \frac{1}{2}\,\boldsymbol{\nu}_{\alpha_{ij}}\mathbf{D}_{\alpha_i}^*\mathbf{D}_{\alpha_j}^* - \mathbf{E}_{\alpha_j}\mathbf{D}_{\alpha_j}^* \end{aligned} \tag{B.2}$$

The first term of the electrostatic energy is proportional to the square of the norm of the total electric induction. Weak heterogeneity of the norm of the dielectric induction is supposed at the single crystal scale so that this first term is taken to be constant over a single crystal. Assuming that the polarisation $\mathbf{P}_\alpha$ is the main contribution to the non-dielectric induction $\mathbf{D}_\alpha^*$, the second term is considered to be proportional to P_0^2, so that it is also a constant within a single crystal. The electrostatic energy of a ferroelectric domain is finally written:

$$W_\alpha^E = -\mathbf{E}_\alpha \cdot \mathbf{D}_\alpha^* + \text{constant} \tag{B.3}$$

The elastic energy is usually given by:

$$W_\alpha^{\boldsymbol{\sigma}} = \frac{1}{2}\,\boldsymbol{\sigma}_\alpha : \boldsymbol{\varepsilon}_\alpha^e \tag{B.4}$$

It can be transformed as follows:

$$\begin{aligned} W_\alpha^{\boldsymbol{\sigma}} &= \frac{1}{2}\,\boldsymbol{\sigma}_{\alpha_{ij}}\boldsymbol{\varepsilon}_{\alpha_{ij}}^e = \frac{1}{2}\,\mathcal{C}_{\alpha_{ijkl}}(\boldsymbol{\varepsilon}_{\alpha_{ij}}-\boldsymbol{\varepsilon}_{\alpha_{ij}}^*)(\boldsymbol{\varepsilon}_{\alpha_{kl}}-\boldsymbol{\varepsilon}_{\alpha_{kl}}^*) \\ &= \frac{1}{2}\,\mathcal{C}_{\alpha_{ijkl}}\boldsymbol{\varepsilon}_{\alpha_{ij}}\boldsymbol{\varepsilon}_{\alpha_{kl}} + \frac{1}{2}\,\mathcal{C}_{\alpha_{ijkl}}\boldsymbol{\varepsilon}_{\alpha_{ij}}^*\boldsymbol{\varepsilon}_{\alpha_{kl}}^* - \mathcal{C}_{\alpha_{ijkl}}\boldsymbol{\varepsilon}_{\alpha_{ij}}\boldsymbol{\varepsilon}_{\alpha_{kl}}^* \\ &= \frac{1}{2}\,\mathcal{C}_{\alpha_{ijkl}}\boldsymbol{\varepsilon}_{\alpha_{ij}}\boldsymbol{\varepsilon}_{\alpha_{kl}} + \frac{1}{2}\,\mathcal{C}_{\alpha_{ijkl}}\boldsymbol{\varepsilon}_{\alpha_{ij}}^*\boldsymbol{\varepsilon}_{\alpha_{kl}}^* - \mathcal{C}_{\alpha_{ijkl}}(\boldsymbol{\varepsilon}_{\alpha_{ij}}^* + \boldsymbol{\varepsilon}_{\alpha_{ij}}^e)\boldsymbol{\varepsilon}_{\alpha_{kl}}^* \\ &= \frac{1}{2}\,\mathcal{C}_{\alpha_{ijkl}}\boldsymbol{\varepsilon}_{\alpha_{ij}}\boldsymbol{\varepsilon}_{\alpha_{kl}} - \frac{1}{2}\,\mathcal{C}_{\alpha_{ijkl}}\boldsymbol{\varepsilon}_{\alpha_{ij}}^*\boldsymbol{\varepsilon}_{\alpha_{kl}}^* - \boldsymbol{\sigma}_{\alpha_{kl}}\boldsymbol{\varepsilon}_{\alpha_{kl}}^* \end{aligned} \tag{B.5}$$

Weak heterogeneity of elastic properties and total strain is supposed at the single crystal scale so that the first term is taken to be constant over a single crystal. In

addition if we assume that the spontaneous ferroelectric strain $\boldsymbol{\varepsilon}_\alpha^{fe}$ is the main contribution to the inelastic strain $\boldsymbol{\varepsilon}_\alpha^*$ at the domain scale, the second term is proportional to λ_0^{fe2} and is then considered to be constant within a single crystal. The elastic energy of a ferroelectric domain is finally written:

$$W_\alpha^E = -\boldsymbol{\sigma}_\alpha : \boldsymbol{\varepsilon}_\alpha^* + \text{constant} \tag{B.6}$$

Appendix C. Identification of the parameter A_s

This appendix details the definition of Eq. (19) for the identification of the parameter A_s. It is a translation to the case of ferroelectrics of the result given in Daniel et al. (2008) for ferromagnetic materials. The definition of A_s is obtained using a simplified description of an – ideal – unstressed bulk isotropic ferroelectric polycrystal. The polycrystal microstructure is seen as an assembly of ferroelectric domains. By opposition to the single crystal, all the possible orientations in space are considered equiprobable, and the domains are randomly distributed. The macroscopic behaviour is then isotropic. In other words the polycrystal anhysteretic behaviour is obtained by considering that a polycrystal is a single crystal for which all space directions are easy axes. For each domain α, $\mathbf{P}_\alpha = P_0\,\boldsymbol{\alpha}$ (Eq. (1)) so that the macroscopic polarisation is written:

$$\mathbf{P} = \frac{1}{V}\int_V \mathbf{P}_\alpha\, dV = P_0 \int_\alpha f_\alpha\, \boldsymbol{\alpha}\, d\alpha \tag{C.1}$$

In the absence of stress, the free energy Eq. (17) reduces to the term $-\mathbf{E}\cdot\mathbf{P}_\alpha$. Using spherical coordinates (writing $\boldsymbol{\alpha} = [\sin\varphi\cos\theta, \sin\varphi\sin\theta, \cos\varphi]$) and choosing an electric field along $\mathbf{z}$-axis ($\mathbf{E} = E\mathbf{z}$), the volume fractions f_α (Eq. (18)) can be written explicitly:

$$f_\alpha = \frac{1}{S}\exp(K\cos\varphi) \tag{C.2}$$

with $K = A_s P_0 E$ and

$$S = \int_\alpha \exp(-A_s W_\alpha)\, d\alpha = \int_\alpha \exp(A_s P_0\, \boldsymbol{\alpha}.\mathbf{E})\, d\alpha = \frac{4\pi\sinh(K)}{K} \tag{C.3}$$

The macroscopic polarisation (Eq. (C.1)) is then given by:

$$\mathbf{P} = P_0\,\frac{K\cosh(K) - \sinh(K)}{K\sinh(K)}\,\mathbf{z} \tag{C.4}$$

This explicit definition of the polarisation curve can be used to define the initial susceptibility χ^0:

$$\chi^0 = \left.\frac{\partial P_z}{\partial E}\right|_{E=0} \tag{C.5}$$

We obtain:

$$\frac{\partial P_z}{\partial E} = A_s P_0^2\,\frac{\sinh^2(K) - K^2}{K^2\sinh^2(K)} \tag{C.6}$$

This result gives the definition of the initial susceptibility when K tends towards 0:

$$\chi^0 = \frac{1}{3}A_s P_0^2 \tag{C.7}$$

The definition of A_s given by Eq. (19) is then obtained.

Appendix D. Calculation of localisation operators

D.1. Mechanical localisation

The calculation of the localisation tensor $\mathcal{B}_\chi^{\boldsymbol{\sigma}}$ requires several intermediate steps. An inclusion problem is considered first. The Eshelby tensor $\mathcal{N}_\chi$ corresponding to this inclusion problem is calculated (Eshelby, 1957). It depends on the shape of the inclusion and on the elastic properties of the infinite medium. The shape of the inclusion is representative for the phase distribution (Bornert et al., 2001). If the grain distribution is isotropic, a spherical inclusion is chosen. In the case of a self-consistent calculation, the elastic stiffness tensor of the infinite medium is the self-consistent estimate $\tilde{\mathcal{C}}_\Omega$. Mura (1982) provides the guidelines for the practical calculation of the Eshelby tensor. The Hill constraint tensor $\mathcal{C}_\chi^*$ is then defined (Eq. (D.1)), from which the strain localisation tensor $\mathcal{A}_\chi^{\boldsymbol{\sigma}}$ (Eq. (D.2)) and the stress concentration tensor $\mathcal{B}_\chi^{\boldsymbol{\sigma}}$ are deduced (Eq. (D.3)). $\mathcal{I}$ is the fourth order identity tensor. The incompatibility tensor $\mathcal{L}_\chi^{\boldsymbol{\sigma}}$ is finally deduced (Eq. (D.4)).

$$\mathcal{C}_\chi^* = \tilde{\mathcal{C}}_\Omega : \left(\mathcal{N}_\chi{}^{-1} - \mathcal{I}\right) \tag{D.1}$$

$$\mathcal{A}_\chi^{\boldsymbol{\sigma}} = \left(\mathcal{C}_\chi + \mathcal{C}_\chi^*\right)^{-1} : \left(\tilde{\mathcal{C}}_\Omega + \mathcal{C}_\chi^*\right) \tag{D.2}$$

$$\mathcal{B}_\chi^{\boldsymbol{\sigma}} = \mathcal{C}_\chi : \mathcal{A}_\chi^{\boldsymbol{\sigma}} : \tilde{\mathcal{C}}_\Omega^{-1} \tag{D.3}$$

$$\mathcal{L}_\chi^{\boldsymbol{\sigma}} = \left(\mathcal{C}_\chi^{-1} + \mathcal{C}_\chi^{*-1}\right)^{-1} \tag{D.4}$$

D.2. Electric localisation

The same approach applies for the electric field localisation. The depolarising tensor $\mathbf{N}_\chi$ is calculated (see for instance Sihvola (1999) or Milton (2002)). The self consistent estimate $\tilde{\boldsymbol{\epsilon}}_\Omega$ for the dielectric permittivity is also used. The intermediate tensor $\boldsymbol{\epsilon}_\chi^*$, and localisation operators $\mathcal{A}_\chi^E$ and $\mathcal{B}_\chi^E$ are then calculated. $\mathbf{I}$ is the second order identity tensor. The incompatibility tensor $\mathcal{M}_\chi^E$ is finally deduced Eq. (D.8).

$$\boldsymbol{\epsilon}_\chi^* = \tilde{\boldsymbol{\epsilon}}_\Omega : \left(\mathbf{N}_\chi{}^{-1} - \mathbf{I}\right) \tag{D.5}$$

$$\mathcal{A}_\chi^E = \left(\boldsymbol{\epsilon}_\chi + \boldsymbol{\epsilon}_\chi^*\right)^{-1} : \left(\tilde{\boldsymbol{\epsilon}}_\Omega + \boldsymbol{\epsilon}_\chi^*\right) \tag{D.6}$$

$$\mathcal{B}_\chi^E = \boldsymbol{\epsilon}_\chi : \mathcal{A}_\chi^E : \tilde{\boldsymbol{\epsilon}}_\Omega^{-1} \tag{D.7}$$

$$\mathcal{M}_\chi^E = \left(\boldsymbol{\epsilon}_\chi + \boldsymbol{\epsilon}_\chi^*\right)^{-1} \tag{D.8}$$

A detailed explanation for the definition of scale transition rules in the case of coupled behaviour can be found in Corcolle et al. (2008).

Appendix E. Role of local elastic anisotropy

The contribution of elastic anisotropy at the single crystal scale to the overall behaviour of ferroelectric ceramics is often neglected, because of its supposed negligible contribution compared to domain switching (Kamlah et al., 2005). This appendix aims at a quantitative evaluation of the influence of local elastic anisotropy for PZT.

We consider the PZT isotropic polycrystal with macroscopic Young's modulus E_Ω and Poisson's ratio ν_Ω. These properties can be expressed in terms of shear modulus μ_Ω and bulk modulus k_Ω:

$$\mu_\Omega = \frac{E_\Omega}{2(1+\nu_\Omega)} \quad \text{and} \quad k_\Omega = \frac{E_\Omega}{3(1-2\nu_\Omega)} \tag{E.1}$$

Several values of local elastic anisotropy can lead to the same macroscopic properties. We consider a single crystal with cubic symmetry. The elastic properties of the single crystal obey the cubic symmetry and are given by two shear moduli $\mu_\chi^{\mathbf{a}}$ and $\mu_\chi^{\mathbf{b}}$ and a bulk modulus k_χ (Eq. (E.2)). The anisotropy ratio r is defined by Eq. (E.3).

$$\begin{cases} \mu_\chi^{\mathbf{a}} = \frac{1}{2}(\mathcal{C}_{\chi 1111} - \mathcal{C}_{\chi 1122}) \\ \mu_\chi^{\mathbf{b}} = \mathcal{C}_{\chi 2323} \\ k_\chi = \frac{1}{3}(\mathcal{C}_{\chi 1111} + 2\mathcal{C}_{\chi 1122}) \end{cases} \tag{E.2}$$

$$r = \frac{\mu_\chi^{\mathbf{a}}}{\mu_\chi^{\mathbf{b}}} \tag{E.3}$$

The effective isotropic elastic properties are then given by the effective shear modulus $\tilde{\mu}_\Omega$ and bulk modulus $\tilde{k}_\Omega$ (Bornert et al., 2001).

$$\tilde{\mu}_\Omega = \frac{5\left(\mu_\chi^{\mathbf{a}} + \mu^*\right)\left(\mu_\chi^{\mathbf{b}} + \mu^*\right)}{3\mu_\chi^{\mathbf{a}} + 2\mu_\chi^{\mathbf{b}} + 5\mu^*} - \mu^* \tag{E.4}$$

$$\tilde{k}_\Omega = k_\chi \tag{E.5}$$

μ^* is the shear modulus of the Hill Constraint tensor given by Eq. (E.6) (the compressibility k^* of the Hill constraint tensor is given by $3k^* = 4\mu^\infty$).

$$2\mu^* = \frac{\mu^\infty(9k^\infty + 8\mu^\infty)}{3(k^\infty + 2\mu^\infty)} \tag{E.6}$$

μ^∞ and k^∞ are respectively the shear and bulk modulus of the isotropic infinite medium chosen for the Eshelby inclusion problem (Bornert et al., 2001). If the self consistent scheme is chosen, $\mu^\infty = \tilde{\mu}_\Omega$ and $k^\infty = \tilde{k}_\Omega$. Using the self-consistent model in Eq. (E.4), for given macroscopic properties E_Ω and ν_Ω, and for a given local anisotropy ratio r, the local elastic properties are given by:

$$\begin{cases} \mu_\chi^{\mathbf{b}} = \frac{1}{2}(\Gamma + \sqrt{\Delta}) \\ \mu_\chi^{\mathbf{a}} = r\,\mu_\chi^{\mathbf{b}} \\ k_\chi = k_\Omega = \frac{E_\Omega}{3(1-2\nu_\Omega)} \end{cases} \tag{E.7}$$

with

$$\begin{cases} \Gamma = -\left(\frac{2r+3}{5r}\right)\mu^* + \left(\frac{3r+2}{5r}\right)\mu_\Omega \\ \Delta = \left(\frac{2r+3}{5r}\right)^2 \mu^{*2} + \left(\frac{3r+2}{5r}\right)^2 \mu_\Omega^2 - \frac{2(6r^2-37r+6)}{25r^2}\mu^*\mu_\Omega \end{cases} \tag{E.8}$$

It is then possible to define different sets of local elastic coefficients $(\mu_\chi^{\mathbf{a}}, \mu_\chi^{\mathbf{b}}, k_\chi)$ corresponding to different local anisotropy ratio r but leading to the same macroscopic elastic properties (μ_Ω, k_Ω). The influence of local anisotropy can thus be investigated. In the following figures the variation Δp of a parameter p as a function of the elastic anisotropy ratio is defined by Eq. (E.9).

$$\Delta p = 100 \cdot \frac{p(r) - p(r=1)}{p(r=1)} \tag{E.9}$$

Fig. E.11 plots the variation obtained for the single crystal macroscopic response as a function of the single crystal elastic anisotropy. The prediction of the macroscopic electric induction is hardly influenced by the local elastic anisotropy (Fig. E.11(a)) but the prediction of the macroscopic strain is significantly modified. For an anisotropy ratio $r = 2$, the predicted macroscopic strain is 10% higher compared to the strain obtained under the assumption of local elastic isotropy ($r = 1$).

Second order moments of stress are not very sensitive to the level of local anisotropy (Fig. E.12(a)). A few percents of variation are observed on the parameters M_{33} and M_{12} as

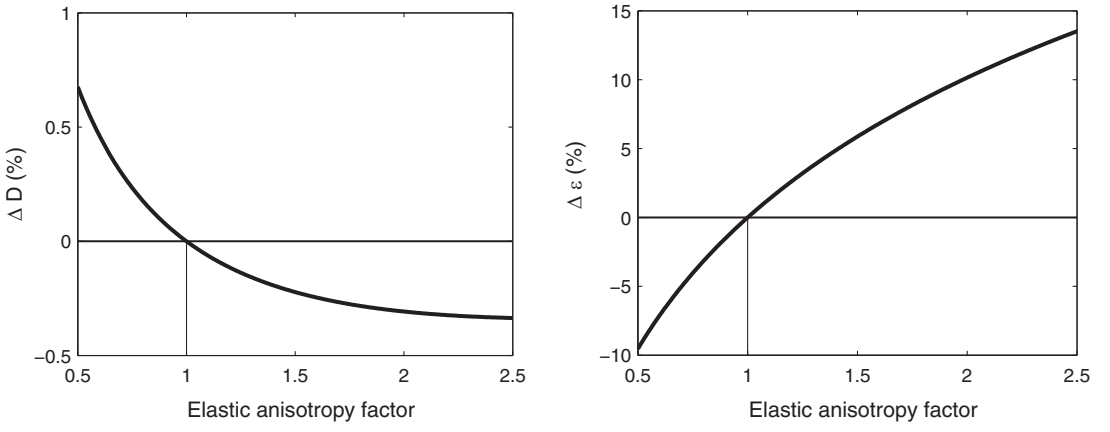

(a) Electric induction (b) Strain

Fig. E.11. Relative variation of electric induction and strain as a function of the single crystal elastic anisotropy ratio r ($E = 1$ MV/mm, no applied stress).

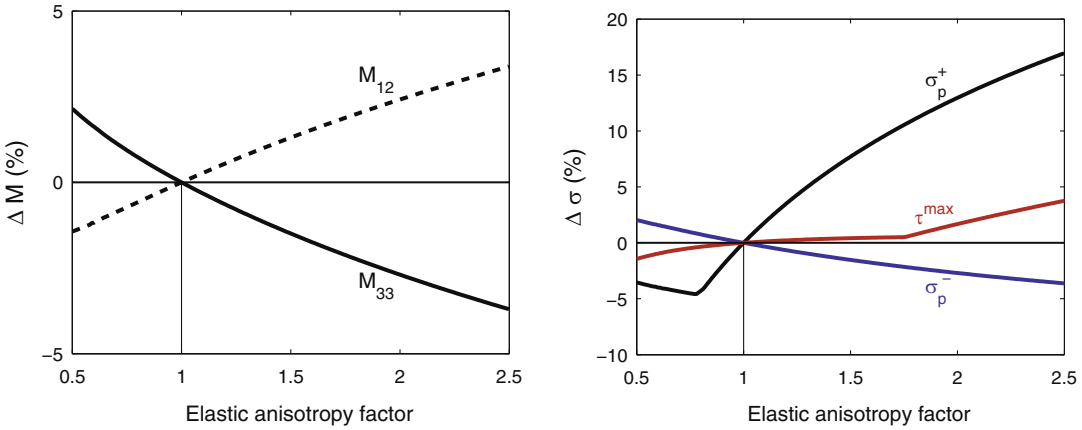

(a) Second order moments (b) Maximum stress

Fig. E.12. Relative variation of second order moments and maximum stress as a function of the single crystal elastic anisotropy ratio r (E = 1 MV/mm, no applied stress).

a function of r, meaning that the variability of stress is of the same order of magnitude whatever the single crystal anisotropy. But maximum stress values significantly depends on the local anisotropy as shown in Fig. E.12(b). For an anisotropy of $r = 2$ the maximum principal stress is increased by 13% compared to the corresponding isotropic single crystal.

It can then be concluded that single crystal elastic anisotropy plays a significant role in the behaviour of ferroelectric materials, particularly concerning macroscopic strain and internal stresses, and should not be neglected in modelling approaches. Results are presented here in the absence of applied stress, but it can be shown that the sensitivity to local elastic anisotropy is even higher when a macroscopic stress is applied (Daniel et al., 2013).

Appendix F. Saturation polarisation and saturation ferroelectric strain of isotropic polycrystals

The saturation state of isotropic polycrystals is a particular state for which the material is a random collection of single crystals fully polarised along the easy direction closest to the applied electric field. Under such conditions the saturation polarisation P_Ω^{sat} and saturation ferroelectric strain λ_Ω^{sat} can be calculated analytically. Uchida and Ikeda (1967) and Li and Rajapakse (2007) give the solution for P_Ω^{sat} and λ_Ω^{sat} under the assumption of uniform stress[1] and uniform electric field within the polycrystal.[2]

For a tetragonal material electrically polarised at saturation, the solutions are given by Eqs. (F.1) and (F.2).

$$P_\Omega^{sat} = \frac{3\sqrt{2}}{\pi}\left(\frac{\pi}{2} - \tan^{-1}\sqrt{2}\right)P_0 \approx 0.831\,P_0 \tag{F.1}$$

$$\lambda_\Omega^{sat} = \frac{\sqrt{3}}{\pi}\lambda_0^{fe} \approx 0.551\,\lambda_0^{fe} \tag{F.2}$$

For a rhombohedral material electrically polarised at saturation, the solutions are given by Eqs. (F.3) and (F.4).

$$P_\Omega^{sat} = \frac{\sqrt{3}}{2}P_0 \approx 0.866\,P_0 \tag{F.3}$$

$$\lambda_\Omega^{sat} = \frac{2}{\pi}\lambda_0^{fe} \approx 0.637\,\lambda_0^{fe} \tag{F.4}$$

These equations can be used to identify P_0 and λ_0^{fe} from macroscopic measurement at saturation – after removing from the strain measurement the piezoelectric contribution proportional to the electric field. They should however be used with care since electric field and stress are not uniform within a polycrystal due to material heterogeneity.

These analytical solutions can also be used to define the minimum number of crystallographic orientations needed to describe an isotropic polycrystal. For that purpose, and for several values of the number N of orientations, 500 different random orientation distribution functions were evaluated. Under uniform stress and uniform electric field hypotheses, saturation polarisation and saturation ferroelectric strain have been calculated and compared to the analytical results of Eqs. (F.1) and (F.2). The results are plotted in Fig. F.13.

For a number of 100 orientations, the obtained value of the saturation polarisation lies in a band of ±4.4% around the theoretical value. For $N = 500$, the band is ±1.8% wide, ±1.1% for $N = 1000$ and ±0.67% for $N = 5000$. The discrete orientation distribution function with 546 orientations obtained by a regular mapping of the crystallographic orientations space (Fig. 3) gives the result with a precision of 0.5%.

The variability is higher for the saturation ferroelectric strain. For a number of 100 orientations, the obtained value lies in a band of ±16% around the theoretical value. For $N = 500$, the band is ±6.5% wide, ±4.0% for $N = 1000$

[1] The macroscopic ferroelectric strain is then the volume average of the local ferroelectric strain.

[2] The macroscopic polarisation is then the volume average of the local polarisation.

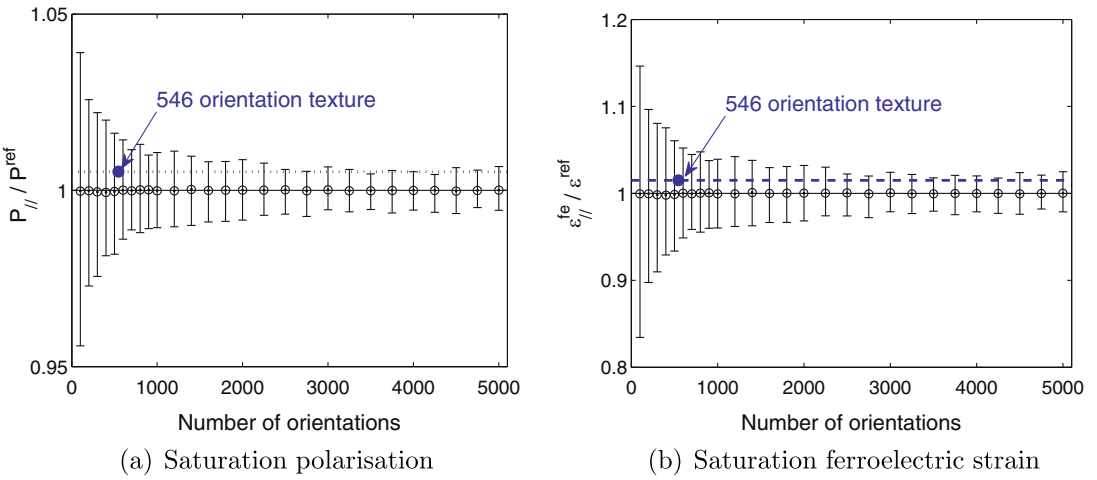

Fig. F.13. Variability obtained on saturation characteristics as a function of the number of orientations in the discrete orientation distribution function (500 random orientation distribution functions for each number N of orientations, the dashed line is the solution obtained with the regular 546 orientation mapping of the crystallographic orientations space – see Fig. 3).

and $\pm 2.5\%$ for $N = 5000$. The discrete orientation distribution function with 546 orientations (Fig. 3) gives the result with a precision of 1.5%.

It can be noticed that the mean value over the 500 random distribution functions leads approximately to the correct value for the saturation polarisation and saturation ferroelectric strain. A solution to get accurate results would be to define a great number of random distribution functions, and to calculate the mean value over the obtained results. However this solution appears to be expensive in terms of computation time. On the other hand the 546 orientation distribution function provides reasonably accurate results with a limited number of orientations. This is the reason why it has been used in the calculations presented in this paper.

References

Arlt, G., 1987. The role of domain walls on the dielectric, elastic and piezoelectric properties of ferroelectric ceramics. Ferroelectrics 76, 451–458.

Arlt, G., 1990. Twinning in ferroelectric and ferroelastic ceramics: stress relief. J. Mat. Sci. 25, 2655–2666.

Arlt, G., Hennings, D., de With, G., 1985. Dielectric properties of fine-grained Barium Titanate ceramics. J. Appl. Phys. 58 (4), 1619–1625.

Armstrong, W.D., 1997. Magnetization and magnetostriction processes in $Tb_{(0.27\text{-}0.30)}$ $Dy_{(0.73\text{-}0.70)}Fe_{(1.9\text{-}2.0)}$. J. Appl. Phys. 81, 2321–2326.

Armstrong, W.D., 2002. A directional magnetization potential based model of magnetoelastic hysteresis. J. Appl. Phys. 91, 2202–2210.

Arockiarajan, A., Menzel, A., Delibas, B., Seeman, W., 2007. Micromechanical modeling of switching effects in piezoelectric materials – a robust coupled finite element approach. J. Intell. Mater. Syst. Struct. 18, 983–999.

Bassiouny, E., Maugin, G.A., 1989. Thermodynamical formulation for coupled electromechanical hysteresis effects – III Parameter identification. Int. J. Eng. Sci. 27, 975–987.

Bassiouny, E., Maugin, G.A., 1989. Thermodynamical formulation for coupled electromechanical hysteresis effects – IV Combined electromechanical loading. Int. J. Eng. Sci. 27, 989–1000.

Bassiouny, E., Ghaleb, A.F., Maugin, G.A., 1988. Thermodynamical formulation for coupled electromechanical hysteresis effects – I basic equations. Int. J. Eng. Sci. 26, 1279–1295.

Bassiouny, E., Ghaleb, A.F., Maugin, G.A., 1988. Thermodynamical formulation for coupled electromechanical hysteresis effects – II Poling of ceramics. Int. J. Eng. Sci. 26, 1297–1306.

Berlincourt, D., 1992. Piezoelectric ceramic compositional development. J. Acoust. Soc. Am. 91, 3034–3040.

Berveiller, M., Zaoui, A., 1978. An extension of the self-consistent scheme to plastically-flowing polycrystals. J. Mech. Phys. Solids 26, 325–344.

Bornert, M., Bretheau, T., Gilormini, P., 2001. Homogénéisation en mécanique des matériaux. Tome 1: Matériaux aléatoires élastiques et milieux périodiques. Hermès Science.

Bozorth, R.M., 1951. Ferromagnetism. Van Nostrand.

Buessem, W.R., Cross, L.E., Goswami, A.K., 1966. Phenomenological theory of high permittivity in fine-grained Barium Titanate. J. Am. Ceram. Soc. 49 (1), 33–36.

Buessem, W.R., Cross, L.E., Goswami, A.K., 1966. Effect of two-dimensional pressure on the permittivity of fine- and coarse-grained Barium Titanate. J. Am. Ceram. Soc. 49 (1), 36–39.

Buiron, N., Hirsinger, L., Billardon, R., 1999. A multiscale model for magneto-elastic couplings. J. Phys. IV 9, 187–196.

Cao, H., Evans, A.G., 1993. Nonlinear deformation of ferroelectric ceramics. J. Am. Ceram. Soc. 76 (4), 890–896.

Chen, L.Q., 2002. Phase-field models for microstructure evolution. Annu. Rev. Mater. Res. 32, 113–140.

Chen, W., Lynch, C., 1998. A micro-electro-mechanical model for polarization switching of ferrroelectric materials. Acta Mater. 46 (15), 5303–5311.

Chen, P.J., Peercy, P.S., 1979. One dimensional dynamic electromechanical constitutive relations of ferroelectric materials. Acta Mech. 31, 231–241.

Choudhury, S., Li, Y.L., Krill, C.E., Chen, L.Q., 2005. Phase-field simulation of polarization switching and domain evolution in ferroelectric polycrystals. Acta Mater. 53 (20), 5313–5321.

Cocks, A.C.F., McMeeking, R.M., 1999. A phenomenological constitutive law for the behaviour of ferroelectric ceramics. Ferroelectrics 228, 219–228.

Corcolle, R., Daniel, L., Bouillault, F., 2008. Generic formalism for homogenization of coupled behaviors: application to magnetoelectroelastic behavior. Phys. Rev. B 78 (21), 214110.

Damjanovic, D., Demartin, M., 1996. The Rayleigh law in piezoelectric ceramics. J. Phys. D: Appl. Phys. 29, 2057–2060.

Damjanovic, D., Brem, F., Setter, N., 2002. Crystal orientation dependence of the piezoelectric d_{33} coefficient in tetragonal $BaTiO_3$ as a function of temperature. Appl. Phys. Lett. 80, 652–654.

Daniel, L., Hubert, O., Buiron, N., Billardon, R., 2008. Reversible magneto-elastic behavior: a multiscale approach. J. Mech. Phys. Solids 56, 1018–1042.

Daniel, L., Hall, D.A., Withers, P.J., 2013. Analysis of the contribution of elastic anisotropy to internal stresses in ferroelectric materials using a multiscale modelling approach. In: Proceedings of the Electroceramics for End-users VII Conference (PIEZO 2013), Les Arcs, France, 2013.

Du, X.H., Zheng, J., Belegundu, U., Uchino, K., 1998. Crystal orientation dependence of piezoelectric properties of lead zirconate titanate near the morphotropic phase boundary. Appl. Phys. Lett. 72, 2421–2423.

Elhadrouz, M., Ben Zineb, T., Patoor, E., 2005a. Constitutive law for ferroelastic and ferroelectric piezoceramics. J. Intell. Mater. Syst. Struct. 16, 221–236.
Elhadrouz, M., Ben Zineb, T., Patoor, E., 2005b. Constitutive law for ferroelectric and ferroelastic single crystals: a micromechanical approach. Comput. Mater. Sci. 32, 355–359.
Eshelby, J.D., 1957. The determination of the elastic field of an ellipsoidal inclusion, and related problems. Proc. R. Soc. Lond. A 421, 376–396.
Guo, R., Cross, L.E., Park, S-E., Noheda, B., Cox, D.E., Shirane, G., 2000. Origin of the High Piezoelectric Response in $PbZr_{1-x}Ti_xO_3$. Phys. Rev. Lett. 84, 5423–5426.
Hall, D.A., Stevenson, P.J., 1999. High field dielectric behaviour of ferroelectric ceramics. Ferroelectrics 228, 139–158.
Hall, D.A., Steuwer, A., Cherdhirunkorn, B., Withers, P.J., Mori, T., 2005. Micromechanics of residual stress and texture development due to poling in polycrystalline ferroelectric ceramics. J. Mech. Phys. Solids 53, 249–260.
Haug, A., Huber, J.E., Onck, P.R., Van der Giessen, E., 2007. Multi-grain analysis versus self-consistent estimates of ferroelectric polycrystals. J. Mech. Phys. Solids 55, 648–665.
Hauser, H., 2004. Energetic model of ferromagnetic hysteresis: Isotropic magnetization. J. Appl. Phys. 96 (5), 2753–2767.
Hill, R., 1965. Continuum micro-mechanics of elastoplastic polycrystals. J. Mech. Phys. Solids 13, 89–101.
Hong, S.H., Trolier-McKinstry, S., Messing, G.L., 2000. Dielectric and electromechanical properties of textured niobium-doped bismuth titanate ceramics. J. Am. Ceram. Soc. 83 (1), 113–118.
Huber, J.E., 2005. Micromechanical modelling of ferroelectrics. Curr. Opin. Solid State Mater. Sci. 9, 100–106.
Huber, J.E., Fleck, N.A., 2001. Multi-axial electrical switching of a ferroelectric: theory versus experiment. J. Mech. Phys. Solids 49, 785–811.
Huber, J.E., Fleck, N.A., Landis, C.M., McMeeking, R.M., 1999. A constitutive model for ferroelectric polycrystals. J. Mech. Phys. Solids 47, 1663–1697.
Hubert, A., Schaëfer, R., 1998. Magnetic Domains. Springer, Berlin.
Hwang, S.C., McMeeking, R.M., 1999. A finite element model of ferroelastic polycrystals. Int. J. Solids Struct. 36, 1541–1556.
Hwang, S.C., Lynch, C.S., McMeeking, R.M., 1995. Ferroelectric/ferroelastic interactions and a polarization switching model. Acta Metall. Mater. 43, 2048–2073.
Hwang, S.C., Huber, J.E., McMeeking, R.M., Fleck, N.A., 1998. The simulation of switching in polycrystalline ferroelectric ceramics. J. Appl. Phys. 84, 1530–1540.
Jiles, D.C., 1991. Introduction to Magnetism and Magnetic Materials. Chapman & Hall, London.
Jiles, D.C., Atherton, D., 1984. Theory of ferromagnetic hysteresis. J. Appl. Phys. 55 (6), 2115–2120.
Kamlah, M., Tsakmakis, C., 1999. Phenomenological modeling of the non-linear electro-mechanical coupling in ferroelectrics. Int. J. Solids Struct. 36, 669–695.
Kamlah, M., Wang, Z., 2003. A thermodynamically and microscopically motivated constitutive model for piezoceramics. Comput. Mater. Sci. 28, 409–418.
Kamlah, M., Liskowsky, A.C., McMeeking, R.M., Balke, H., 2005. Finite element simulation of a polycrystalline ferroelectric based on a multidomain single crystal switching model. Int. J. Solids Struct. 42, 2949–2964.
Klinkel, S., 2006. A phenomenological constitutive model for ferroelastic and ferroelectric hysteresis effects in ferroelectric ceramics. Int. J. Solids Struct. 43, 7197–7222.
Landis, C.M., 2002. Fully coupled, multi-axial, symmetric constitutive laws for polycrystalline ferroelectric ceramics. J. Mech. Phys. Solids 50, 127–152.
Landis, C.M., 2004. Non-linear constitutive modeling of ferroelectrics. Curr. Opin. Solid State Mater. Sci. 8, 59–69.
Li, F.X., Fang, D.N., 2004. Simulations of domain switching in ferroelectrics by a three-dimensional finite element model. Mech. Mater. 36, 959–973.
Li, J.Y., Liu, D., 2004. On ferroelectric crystals with engineered domain configurations. J. Mech. Phys. Solids 52, 1719–1742.
Li, F.X., Rajapakse, R.K.N.D., 2007. Analytical saturated domain orientation textures and electromechanical properties of ferroelectric ceramics due to electric/mechanical poling. J. Appl. Phys. 101, 054110.
Li, J., Weng, G.J., 1999. A theory of domain switch for the nonlinear behaviour of ferroelectrics. Proc. R. Soc. Lond. A 455, 3493–3511.
Loge, R.E., Suo, Z., 1996. Nonequilibrium thermodynamics of ferroelectric domain evolution. Acta Mater. 44 (8), 3429–3438.
Lu, W., Fang, D.N., Li, C.Q., Hwang, K.C., 1999. Nonlinear electric-mechanical behavior and micromechanics modelling of ferroelectric domain evolution. Acta Mater. 47 (10), 2913–2926.
McMeeking, R.M., Landis, C.M., 2002. A phenomenological multi-axial constitutive law for switching in polycrystalline ferroelectric ceramics. Int. J. Eng. Sci. 40, 1553–1577.
Mehling, V., Tsakmakis, C., Gross, D., 2007. Phenomenological model for the macroscopical material behavior of ferroelectric ceramics. J. Mech. Phys. Solids 55, 2106–2141.
Michelitsch, T., Kreher, W.S., 1998. A simple model for the nonlinear material behavior of ferroelectrics. Acta Mater. 46 (14), 5085–5094.
Milton, G.W., 2002. The Theory of Composites. Cambridge University Press, New York.
Mura, T., 1982. Micromechanics of Defects in Solids. Martinus Nijhoff Publishers, Dordrecht, MA.
Noheda, B., Cox, D.E., Shirane, G., Gonzalo, J.A., Cross, L.E., Park, S-E., 1999. A monoclinic ferroelectric phase in the $Pb(Zr_{1-x}Ti_x)O_3$ solid solution. Appl. Phys. Lett. 74, 2059–2061.
Pathak, A., McMeeking, R.M., 2008. Three-dimensional finite element simulations of ferroelectric polycrystals under electrical and mechanical loading. J. Mech. Phys. Solids 56, 663–683.
Pearson, J., Squire, P.T., Atkinson, D., 1997. Which anhysteretic magnetization curve? IEEE Trans. Magn. 33 (5), 3970–3972.
Potnis, P.R., Tsou, N.T., Huber, J.E., 2011. A review of domain modelling and domain imaging techniques in ferroelectric crystals. Materials 4, 417–447.
Pramanick, A., Damjanovic, D., Daniels, J.E., Nino, J.C., Jones, J.L., 2011. Origins of electro-mechanical coupling in polycrystalline ferroelectrics during subcoercive electrical loading. J. Am. Ceram. Soc. 94 (2), 293–309.
Rödel, J., 2007. Effective intrinsic linear properties of laminar piezoelectric composites and simple ferroelectric domain structures. Mech. Mater. 39, 302–325.
Rödel, J., Kreher, W.S., 2000. Self-consistent modelling of non-linear effective properties of polycrystalline ferroelectric ceramics. Comput. Mater. Sci. 19, 123–132.
Rödel, J., Jo, W., Seifert, K.T.P., Anton, E.M., Granzow, T., 2009. Perspective on the development of lead-free piezoceramics. J. Am. Ceram. Soc. 92 (6), 1153–1177.
Saito, Y., Takao, H., Tani, T., Nonoyama, T., Takatori, K., Homma, T., Nagaya, T., Nakamura, M., 2004. Lead-free piezoceramics. Nature 432, 84–87.
Schönau, K.A., Knapp, M., Kungl, H., Hoffmann, M.J., Feuss, H., 2007. In situ synchrotron diffraction investigation of morphotropic $Pb[Zr_xTi_{1-x}]O_3$ under an applied electric field. Phys. Rev. B 76, 144112.
Shilo, D., Burcsu, E., Ravichandran, G., Bhattacharya, K., 2007. A model for large electrostrictive actuation in ferroelectric single crystals. Int. J. Solids Struct. 44, 2053–2065.
Sihvola, A., 1999. Electromagnetic mixing formulas and applications. IEE Electromagnetic Waves Series, vol. 47, 1999.
Su, Y., Landis, C.M., 2007. Continuum thermodynamics of ferroelectric domain evolution: theory, finite element implementation, and application to domain wall pinning. J. Mech. Phys. Solids 55, 280–305.
Tang, W., Fang, D.N., Li, J.Y., 2009. Two-scale micromechanics-based probabilistic modeling of domain switching in ferroelectric ceramics. J. Mech. Phys. Solids 57, 1683–1701.
Tsou, N.T., Huber, J.E., 2010. Compatible domain structures and the poling of single crystal ferroelectrics. Mech. Mater. 42, 740–753.
Uchida, N., Ikeda, T., 1967. Electrostriction in Perovskite-type ferroelectric Ceramics. Jpn. J. Appl. Phys. 6 (9), 1079–1088.
Weng, G.J., Wong, D.T., 2009. Thermodynamic driving force in ferroelectric crystals with a rank-2 laminated domain pattern, and a study of enhanced electrostriction. J. Mech. Phys. Solids 57, 571–597.
Yen, J.H., Shu, Y.C., Shieh, J., Yeh, J.H., 2009. A study of electromechanical switching in ferroelectric single crystals. J. Mech. Phys. Solids 57, 1683–1701.
Zhang, Y., Xu, R., Liu, B., Fang, D., 2012. An electromechanical atomic-scale finite element method for simulating evolutions of ferroelectric nanodomains. J. Mech. Phys. Solids 60, 1383–1399.